Observables of spheroidal magnetized strange stars

D. Alvear Terrero [1,*] S. López Pérez [1,†] D. Manreza Paret [2,‡] A. Pérez Martínez [1,§] and G. Quintero Angulo [2,‖]

[1]*Instituto de Cibernética, Matemática y Física, Calle E esq a 15, Vedado 10400, La Habana Cuba*

[2]*Facultad de Física, Universidad de la Habana, San Lázaro y L, Vedado, La Habana 10400, Cuba*

(Received 19 October 2020; accepted 2 April 2021; published 21 April 2021)

We study stable spheroidal configurations of magnetized strange stars using an axially symmetric metric in spherical coordinates that uses a gamma parameter to link the anisotropy in the equation of state due to the magnetic field with the deformation of the star. The stars are composed by magnetized strange quark matter described within the framework of the MIT bag model. Their masses, radii, eccentricity, redshift and mass quadrupole moment are computed. Results are compared with spherical strange star solutions obtained with Tolman-Oppenheimer-Volkoff equations and observational data of strange star candidates. In the spheroidal model the observables depend directly on the deformation of the star, and, even though it is small, the observables strongly deviate from the corresponding spherical configurations. Thus, the highest values of the mass quadrupole moment correspond to the intermediate mass regime. These differences might allow us to discriminate between models with and without magnetic field when compared with observations.

DOI: 10.1103/PhysRevC.103.045807

I. INTRODUCTION

The core of neutron stars (NSs) reach densities beyond that of nuclear saturation ($n_0 = 0.16$ fm^{-3}), which may induce phase transitions from hadronic to quark matter. There are at least two possible quark-related phases within a NS: (a) coexisting hadronic and quark matter at a finite transition pressure and (b) strange quark matter, which is speculated to be the true ground state of strongly interacting matter (Bodmer-Witten's conjecture) [1,2].

Experimentally, the quark-gluon plasma, in the limit of high temperatures and low densities, has been explored in the Relativistic Heavy Ion Collider (RHIC) at Brookhaven National Laboratory (BNL) and in the Large Hadron Collider (LHC) at CERN. Meanwhile, the opposite regime of low temperatures and high densities will be studied in two experimental facilities that are currently under construction, the Facility for Antiproton and Ion Research (FAIR) at GSI and the Nuclotron-based Ion Collider Facility (NICA) at JINR. Nevertheless, since NSs might be the natural habitat for quark matter in the latter regime, the properties of matter under those conditions could also be inferred through astronomical observations.

If the Bodmer-Witten conjecture holds, a hadronic star would only be possible in a long metastable state, eventually decaying into self-bounded strange stars (SSs) [3,4]. Otherwise, hybrid stars [5,6], combining hadrons and quarks, are conceivable as a fully stable constituent of a NS.

SSs models are interesting because they describe compact objects with maximum masses around $1.5M_\odot$ and radius of 4–8 km that could account for some observations of cold, dense, and small compact objects (COs) that do not fit the standard NSs models (see Table I) [7–13]. There are many microscopic models proposed for SSs, all of which differ by how the strong interaction is described and what sort of SQM phases are considered within the star [14].

On the other hand, hybrid stars have received a lot of attention because they can reach $2M_\odot$, which is a robust observational constraint on NSs masses [15].[1] Recently, these models have gained a new support due to the works by Annala *et al.* [17], where a wide set of theoretical equation of states (EoSs) from particle and nuclear physics is compared with benchmark results stemming from gravitational wave (GW) measurements of NS collisions. According to their results, a star with mass $\approx 2M_\odot$ and radius ≈ 12 km is more likely to have a quark core of approximately 6.5 km, than to be formed exclusively by baryons.

The study of SSs starts by seeking the SQM EoS. Inside SSs quarks might be unpaired or paired forming a color superconductor state [19]. However, so far there are neither *ab initio* nor perturbative QCD calculations that lead to the desired EoS in the regime of high densities and zero temperature [20]. Consequently, SQM inside COs is usually described through phenomenological models that mimic the main features of QCD [20]. One of the most used is the MIT bag model [21],

*dianaalvear@icimaf.cu
†samantha@icimaf.cu
‡dmanreza@fisica.uh.cu
§aurora@icimaf.cu
‖gquintero@fisica.uh.cu

[1]Some hadronic models can explain objects with more than $2M_\odot$ (see Ref. [16] and references therein).

TABLE I. Masses M and radii R for observed candidates of SSs.

Observed object	M ($M_\odot$)	R (km)
HerX-1	$1.73^{+0.358}_{-0.173}$ [13]	8.10 ± 0.41[a] [9]
4U1608-52	1.74 ± 0.14 [10]	9.30 ± 1.00 [10]
4U1820-30	1.58 ± 0.06 [11]	9.10 ± 0.40 [11]
4U1538-52	1.02 ± 0.17 [18]	7.866 ± 0.210[a] [9]
SMC X-1	1.21 ± 0.12 [18]	8.831 ± 0.09[a] [9]
LMC X-4	1.57 ± 0.11 [18]	8.301 ± 0.200[a] [9]
Cen X-3	1.57 ± 0.16 [18]	9.178 ± 0.130[a] [9]

[a]The radii are obtained considering the masses as cited in Ref. [9], with a specific model for strange stars so they must be considered as estimated values.

where quarks are considered as quasifree particles confined into a "bag" and having fixed masses. This model reproduces confinement and asymptotic freedom with the use of only one external parameter, the bag energy $\mathtt{B_{Bag}}$.

On the other hand, compact objects have extreme magnetic fields [22]. The observed surface magnetic fields in neutron stars are in the range of 10^9–10^{15} G [23,24], while their inner magnetic fields are estimated to be as high as 5×10^{18} G [20,25]. As is well known, the energy-momentum tensor of matter under a magnetic field is anisotropic [19], a feature that can be interpreted as the gas exerting different pressures in the parallel and perpendicular directions with respect to the magnetic axis [26], and that leads to nonspherical stars [27–30]. To model the structure of magnetized COs, we have previously used the Tolman-Oppenheimer-Volkoff (TOV) equations independently for each pressure [31–34], and an approximate solution of Einstein's equations for an axially symmetric metric in cylindrical coordinates [20]. This leads to the description of two different stellar sequences (one for each pressure), which prevents us from calculating the total mass of the star. That is why, as an attempt to properly describe the macroscopic structure of magnetized COs, we derived a set of TOV-like structure equations from an axially symmetric metric in spherical coordinates, the γ equations [30], that allow us to describe spheroidal objects as long as their shape is nearly spherical. These equations have been used to model white dwarfs [30], the hypothetical magnetized BEC stars [35] and, preliminary, strange stars [34].

In this paper we return to SSs [31,32,34], emphasizing the magnetic-field effects on the stability of the SQM and the spheroidal stellar configurations. In addition, we compute the eccentricity, the redshift, and the mass quadrupole moment and compare them with those of spherical strange stars. This study is the starting point of a more ambitious project related to the study of magnetized hybrid stars.

In Sec. II we analyze the stability of magnetized SQM in astrophysical conditions and its dependence on the density, the bag energy and the magnetic field. Besides, we revisited the magnetized EoS for SSs and discuss the magnetic-field effects on the energy density and pressures. The γ equations are presented in Sec. III with their corresponding numerical results for magnetized strange stars. Section IV is devoted to the computation of the redshift and the mass quadrupole moment. Concluding remarks are given in Sec. V.

II. EQUATION OF STATE OF MAGNETIZED STRANGE STARS

We consider SSs composed of SQM and electrons under the action of a uniform and constant magnetic field oriented in the z direction, $\mathbf{B} = (0, 0, B)$. This approximation for the magnetic field is reasonable for the construction of the EoS since the characteristic variation length of the macroscopic magnetic field is much larger than the microscopic magnetic scale [36]. The global configuration of a neutron star's magnetic field is much more complex, since it is known that purely poloidal or toroidal fields are unstable and, therefore, realistic stars should be constructed with mixed fields [37,38]. Nevertheless, in this work, we assume a pure poloidal configuration (uniform inside the star) for the magnetic field of the SSs as a first approximation to show how the magnetic field modifies the observables of the stars. This allows us to make direct connections between its microscopic and macroscopic effects on the stars and contribute to an easier physical understanding of our results in a way that could be enlightening when working with more complex magnetic-field configurations.

As pointed out before, we use the phenomenological MIT bag model [21], where quarks are considered as quasifree particles confined to a "bag" that reproduces the asymptotic freedom and confinement through the $\mathrm{B_{bag}}$ parameter, a binding energy which is added to the quark energy and subtracted from their pressure [21]. In this case, we fix the quark masses and charges to $m_u = m_d = 5$ MeV, $m_s = 150$ MeV, $m_e = 0.51$ MeV, $e_u = \frac{2}{3}e$, and $e_d = e_s = -\frac{1}{3}e$.

For a magnetized gas of quarks and electrons, the pressure and the energy density are obtained from the thermodynamical potential [31]

$$\Omega_f(B, \mu_f, T) = -e_f d_f BT \int_{-\infty}^{\infty} \frac{dp_3}{4\pi^2} \sum_{l=0}^{\infty} g_l \times \sum_{p_4} \ln\left[(p_4 + i\mu_f)^2 + \varepsilon_{lf}^2\right], \quad (1)$$

where l stands for the Landau levels and $f = e, u, d, s$ for the electrons and each quark flavor; d_f is the flavor degeneracy factor[2] and $g_l = 2 - \delta_{l0}$ includes the spin degeneracy of the

[2]$d_e = 1$ and $d_u, d_d, d_s = 3$.

fermions for $l \neq 0$. The sum over p_4 corresponds to Matsubara frequencies $p_4 = T(2n+1)\pi$, with $n = 0, \pm1, \pm2, \ldots$. Moreover, T is the absolute temperature, while μ_f, m_f, and e_f are the chemical potential, the mass and the charge of each particle, respectively. The spectrum of charged fermions coupled to a magnetic field is $\varepsilon_{lf} = (p_3^2 + 2|e_f B|l + m_f^2)^{1/2}$ [31].

Equation (1) can be divided in two contributions:

$$\Omega_f(B, \mu_f, T) = \Omega_f^{\rm vac}(B, 0, 0) + \Omega_f^{\rm st}(B, \mu_f, T), \tag{2}$$

with

$$\Omega_f^{\rm vac}(B, 0, 0) = -\frac{e_f d_f B}{2\pi^2} \int_0^\infty dp_3 \sum_{l=0}^{\infty} g_l \varepsilon_{lf}, \tag{3}$$

$$\Omega_f^{\rm st}(B, \mu_f, T) = -\frac{e_f d_f B T}{2\pi^2} \int_0^\infty dp_3 \times \sum_{l=0}^{\infty} g_l \ln[1 + e^{-\beta(\varepsilon_{lf} \pm \mu_f)}]. \tag{4}$$

The vacuum contribution (3) does not depend on the chemical potential nor on the temperature and presents an ultraviolet divergence that must be renormalized [39], in the strong-field approximation ($B \gg B_f^c$), the result is

$$\Omega_f^{\rm vac\ S}(B, 0, 0) = \frac{d_f m_f^4}{24\pi^2} \left(\frac{B}{B_f^c}\right)^2 \ln \frac{B}{B_f^c}, \tag{5}$$

while in the weak field ($B \ll B_f^c$) we have [40]

$$\Omega_f^{\rm vac\ W}(B, 0, 0) = -\frac{d_f m_f^4}{90(2\pi)^2} \left(\frac{B}{B_f^c}\right)^4. \tag{6}$$

In Eqs. (5) and (6), $B_f^c = m_f^2/e_f$ is the critical magnetic field.[3] For electrons $B_e^c \approx 10^{13}$ G while for quarks up, down, and strange we have $B_u^c \approx 10^{15}$ G, $B_d^c \approx 10^{16}$ G, and $B_s^c \approx 10^{19}$ G, respectively.

COs have temperatures much smaller than the Fermi temperature of the gases that compose them [14]. Hence, a good approximation is to compute the thermodynamical potential of these gases in the degenerate limit (T → 0) [14,22]. In that case, the statistical part of the thermodynamical potential becomes

$$\Omega_f^{\rm st}(B, \mu_f, 0) = -\frac{e_f d_f B}{2\pi^2} \int_0^\infty dp_3 \times \sum_{l=0}^{\infty} g_l (\mu_f - \varepsilon_{lf}) \Theta(\mu_f - \varepsilon_{lf}), \tag{7}$$

where $\Theta(\zeta)$ is the unit step function. From Eq. (7), we obtain

$$\Omega_f^{\rm st}(B, \mu_f, 0) = -\frac{e_f d_f B}{4\pi^2} \sum_0^{l_{\rm max}} g_l \left[\mu_f p_f^l - \left(\varepsilon_f^l\right)^2 \ln\left(\frac{\mu_f + p_f^l}{\varepsilon_f^l}\right)\right], \tag{8}$$

where $p_f^l = [\mu_f^2 - (\varepsilon_f^l)^2]^{1/2}$ is the fermi momentum of the particles, $\varepsilon_f^l = (m_f^2 + 2qBl)^{1/2}$ their ground-state energies, and $l_{\rm max} = I[\frac{\mu_f^2 - m_f^2}{2e_f B}]$ the maximum number of occupied Landau levels for fixed magnetic field and chemical potentials. $I[z]$ denotes the integer part of z.

Due to the high fermionic densities inside the stars, the vacuum contribution Eq. (5) is negligible with respect to the statistical one (8) [19].

To illustrate this fact, we fixed the baryonic density and the magnetic field to $n_B = 5n_0$ and $B = 5 \times 10^{17}$ G, respectively, in order to compare $\Omega^{vac}(B, 0, 0) = \sum_f \Omega_f^{vac}(B, 0, 0)$ with $\Omega^{\rm st}(B, \mu_f, 0) = \sum_f \Omega_f^{\rm st}(B, \mu_f, 0)$. The contribution to the vacuum of the electrons and quarks up and down has to be evaluated using the strong magnetic-field approximation while the s quarks are in the weak magnetic-field one. The numerical values show that $\Omega^{\rm vac}(B, 0, 0) \approx 0.07\,{\rm MeV/fm^3}$ is much smaller than $\Omega^{\rm st}(B, \mu_f, 0) \approx 232\,{\rm MeV/fm^3}$. Hence, Eq. (2) is led by the statistical contribution (4) and $\Omega_f(B, \mu_f, 0) = \Omega_f^{\rm st}(B, \mu_f, 0)$. From this point forward the *st* superindex will be neglected.

Strange quark matter inside the star must be in stellar equilibrium [31]. So, we impose β equilibrium, charge neutrality, and baryon number (n_B) conservation to the system in terms of the particle densities $N_f = -\partial\Omega_f/\partial\mu_f$ and the chemical potentials. These conditions read [31]

$$\mu_u + \mu_e - \mu_d = 0, \quad \mu_d - \mu_s = 0, \tag{9a}$$

$$\sum_f e_f N_f = 0, \quad \sum_{i=u,d,s} N_i = 3n_B. \tag{9b}$$

With these considerations, the magnetized SSs EoSs are

$$E = \sum_f [\Omega_f + \mu_f N_f] + B_{\rm bag} + \frac{B^2}{8\pi}, \tag{10a}$$

$$P_\parallel = -\sum_f \Omega_f - B_{\rm bag} - \frac{B^2}{8\pi}, \tag{10b}$$

$$P_\perp = -\sum_f [\Omega_f + B\mathcal{M}_f] - B_{\rm bag} + \frac{B^2}{8\pi}, \tag{10c}$$

where $\mathcal{M}_f = -\partial\Omega_f/\partial B$ is the magnetization. In Eqs. (10) we can easily identify three different contributions. The first one is given by the sum over the thermodynamical quantities of the species and corresponds to the statistical contribution of each kind of particle. In the case of the perpendicular pressure (10c), this term includes a contribution that comes from the particle magnetization: $-B\mathcal{M}_f$ [41]. The second terms in the EoS, $\pm B_{\rm bag}$, are those ensuring asymptotic freedom and confinement for quarks [2,20]. Finally, the last terms in Eqs. (10) are the magnetic-field pressures and energy density $P_\perp^B = E^B = -P_\parallel^B = B^2/8\pi$ [19], or Maxwell contribution. These terms are included since they also participate in the gravitational stability of the star.

[3]The magnetic field at which the cyclotron energy of the particles is comparable to their rest mass. For electrons this is the so-called Schwinger field.

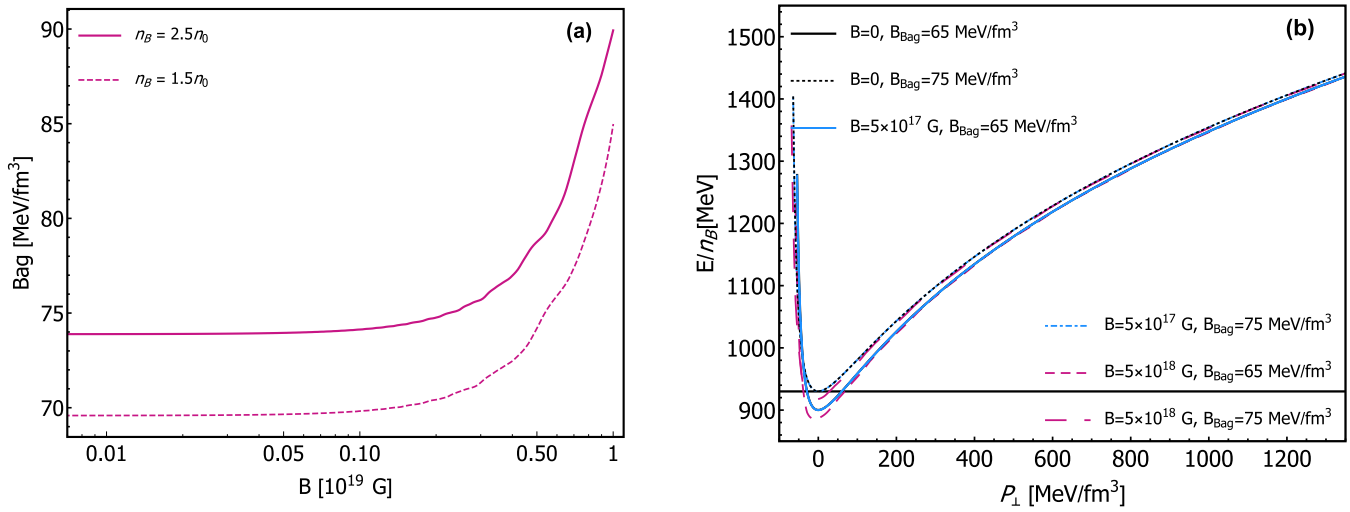

FIG. 1. (a) Stability window for magnetized SQM in the plane **B** vs $\mathtt{B}_{\mathtt{Bag}}$ for fixed values of baryon density n_B/n_0, taking $n_0 = 0.16$ fm^{-3}. (b) Energy per baryon (E/n_B) as a function of the perpendicular pressure ($P_\perp$) at $B = [0, 5 \times 10^{17}, 10^{18}]$ G and for fixed values of the $\mathtt{B}_{\mathtt{Bag}} = [65, 75]$ MeV/fm^3.

Equations (10) allow us to analyze the influence of the magnetic field in the stability of SQM, so that

$$\left.\frac{E}{n_B}\right|^{B}_{\rm SQM} < \left.\frac{E}{n_B}\right|^{B=0}_{\rm SQM} < \left.\frac{E}{n_B}\right|_{\rm Fe^{56}} = 930\ \text{MeV}, \tag{11}$$

is fulfilled inside the star. Fixing $E/n_B|^{B}_{\rm SQM} = 930$ MeV leads us to the stability window of SQM in the plane **B** vs $\mathtt{B}_{\mathtt{Bag}}$. This is shown in the Fig. 1(a), where the SQM is stable for the pairs of B vs $\mathtt{B}_{\mathtt{Bag}}$ below the curves and unstable otherwise. We can also see from this plot that increasing the magnetic field and the baryon density augments the stability region. So, we can say that magnetic-field contributes to stabilize SQM with respect to nuclear matter in astrophysical environments, favoring the existence of SSs. This conclusion is reinforced by the results shown in Fig. 1(b), which illustrates the energy per baryon as a function of the perpendicular pressure. At $P_\perp = 0$, $E/n_B|^{B}_{\rm SQM} < E/n_B|_{\rm Fe^{56}}$, i.e., the magnetic field increases the stability region, while the $\mathtt{B}_{\mathtt{Bag}}$ diminishes it.

A more detailed stability analysis should take into account the $\mathtt{B}_{\mathtt{Bag}}$ dependency with the magnetic field and the baryon density [19]. Nevertheless, the theoretical attempts to find those dependencies or to constrain the $\mathtt{B}_{\mathtt{Bag}}$ values are yet inconclusive and very model dependent [20]. Therefore, in what follows we take $\mathtt{B}_{\mathtt{Bag}}$ as an independent external parameter and study SSs for two fixed, and reasonable, values of it: 65 and 75 MeV/fm^3.

The SQM EoS obtained for those values of $\mathtt{B}_{\mathtt{Bag}}$ at $B = [0, 5 \times 10^{17}, 10^{18}]$ G are depicted in Fig. 2. Note that at higher values of the magnetic field, the difference between the perpendicular and parallel pressures is more appreciable. On the other hand, for a fixed B, the pressures decrease when increasing the $\mathtt{B}_{\mathtt{Bag}}$. These effects on the EoS will be reflected in the macroscopic structure of the star, as we will see in the next section.

III. MAGNETIZED STRANGE STARS: MASS AND RADII

The axial symmetry imposed in the star by the magnetic field is irreconcilable with the spherical symmetry of standard TOV equations. Consequently, it is desirable to use of axisymmetric metrics if one wishes to describe the structure of magnetized COs (see Ref. [30] and references therein). Here, we follow and use a set of axisymmetric structure equations derived from the so-called γ metric [30]:

$$ds^2 = -[1 - 2M(r)/r]^{\gamma} dt^2 + [1 - 2M(r)/r]^{-\gamma} dr^2 + r^2 \sin\theta d\phi^2 + r^2 d\theta^2, \tag{12}$$

where $\gamma = z/r$ accounts for the deformation of the matter source with respect to the spherical shape and parametrizes the polar radius z in terms of the equatorial radius r.

Starting from this metric and considering the anisotropic energy-momentum tensor of magnetized matter, the following structure equations are obtained [30]:

$$\frac{dM}{dr} = 4\pi r^2 \frac{(E_\parallel + E_\perp)}{2}\gamma, \tag{13a}$$

$$\frac{dP_\parallel}{dz} = \frac{1}{\gamma}\frac{dP_\parallel}{dr} = -\frac{(E_\parallel + P_\parallel)\left[\frac{r}{2} + 4\pi r^3 P_\parallel - \frac{r}{2}\left(1 - \frac{2M}{r}\right)^{\gamma}\right]}{\gamma r^2 \left(1 - \frac{2M}{r}\right)^{\gamma}}, \tag{13b}$$

$$\frac{dP_\perp}{dr} = -\frac{(E_\perp + P_\perp)\left[\frac{r}{2} + 4\pi r^3 P_\perp - \frac{r}{2}\left(1 - \frac{2M}{r}\right)^{\gamma}\right]}{r^2 \left(1 - \frac{2M}{r}\right)^{\gamma}}. \tag{13c}$$

This system of equations describe the variation of the mass and the pressures with the spatial coordinate r for an anisotropic axially symmetric CO as long as the parameter γ is close to one [30,42]. Note that they are coupled through the dependence with the energy density and the mass. To solve Eqs. (13), one starts from a point in the star's center with $\mathcal{E}_c = E(r = 0)$, $P_{\parallel_c} = P_\parallel(r = 0)$, and $P_{\perp_c} = P_\perp(r = 0)$,

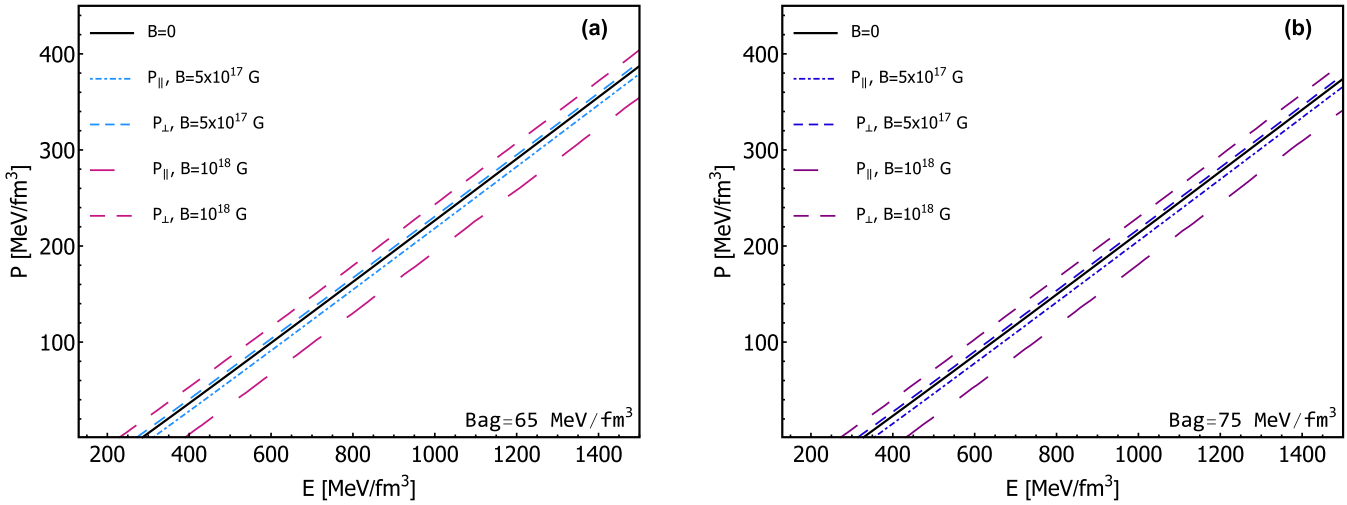

FIG. 2. EoS for magnetized SSs at $B = [0, 5 \times 10^{17}, 10^{18}]$ G. (a) $\mathrm{B_{Bag}} = 65\,\mathrm{MeV/fm^3}$. (b) $\mathrm{B_{Bag}} = 75\,\mathrm{MeV/fm^3}$.

taken from the EoS, and ends the integration at $P_\parallel(Z) = 0$ and $P_\perp(R) = 0$, the conditions that define the radii of the star. But before doing so, one should deal with the fact that γ is a free parameter that cannot be obtained from Eqs. (13). To overcome this difficulty, in Ref. [30] we proposed the ansatz $\gamma = P_{\parallel_c}/P_{\perp_c}$, which connects the geometry of the system with the anisotropy produced by the magnetic field. This interpretation of γ is based on the fact that, for spherical stars a lower central pressure leads to a smaller radius for a fixed central energy density, together with the relation $\gamma = z/r$. This ansatz implies that the shape of the star is only determined by the anisotropy of the EoS in its center and neglects the dependence of the deformation on the pressures inner profiles. In addition, when setting $B = 0$, $P_\perp = P_\parallel$, $\gamma = 1$ and the standard nonmagnetized solution for the structure of COs (TOV equations) is recovered. Therefore, depending on the EoS, the parameter γ will be >1 ($P_{\parallel_c} > P_{\perp_c}$), $=1$ ($P_{\parallel_c} = P_{\perp_c}$), or <1 ($P_{\parallel_c} < P_{\perp_c}$), and the corresponding stars will be prolate, spherical, or oblate, respectively. Moreover, our ansatz inherits the restriction that γ must be close to 1 and this limitation proved to be essential to obtain reasonable results [30].

In Fig. 3 we show the solutions of Eqs. (13) with the use of Eqs. (10) for several values of the magnetic field and the bag energy. They are compared with the nonmagnetized case and with the TOV solutions considering the pairs $(E, P_\perp)$ and $(E, P_\parallel)$ as independent EoS. In the case of TOV solutions, using one EoS or the other leads to different mass-radius relations, whose differences increase with the magnetic field. For a given energy density range, a higher pressure implies bigger and massive stars. Also, for a fixed value of the magnetic field and the $\mathrm{B_{Bag}}$, the difference in the stars size obtained with the pairs $(E, P_\perp)$ and $(E, P_\parallel)$, is larger for heavier stars. This suggest that more massive stars will have a greater deformation. Unlike TOV equations, Eqs. (13) allow us to model the star as a spheroidal with an equatorial radius R and a polar radius Z. So, in Fig. 3 the $M - R$ and $M - Z$ curves correspond to a unique sequence of stars, while the $M - R_\perp$ and the $M - R_\parallel$ curves stand for two different sequences with EoS $(E, P_\perp)$ and $(E, P_\parallel)$, respectively.

The stellar configurations obtained with Eq. (13) are oblate objects ($R > Z$), as expected since $P_\perp > P_\parallel$ (see Figs. 2 and 3). On the contrary of what happens with TOV solutions, for which the difference between $R_\perp$ and $R_\parallel$ increases with the mass, the deformation of our spheroidal stars—the differences between the equatorial and the polar radius—decreases with the mass [34] (see Fig. 3). Hence, the importance of building a model, as the one we present, that takes into account both pressures simultaneously. Note also in Fig. 3 that, in the curves with $B = 5 \times 10^{17}$ G (for $M \leqslant M_\odot$) and $B = 10^{18}$ G, a lower mass corresponds to a bigger equatorial radius. This behavior contradicts the typical proportionality between masses and radii for nonmagnetized strange stars $M \sim R^3$ and, since our structure equations are an approximation to describe almost spherical stars, i.e., stars whose mass-radius behavior are close to that of the $B = 0$ case, it needs further consideration. The dot in the curves at $B = 5 \times 10^{17}$ G denotes the largest value of equatorial radius for which our results are still reasonable and it corresponds to the minimum of the $R(E)$ curve, as will be discussed below.

Figure 4(a) displays the equatorial radius R as a function of the central energy density (E_c) of the stars for $\mathrm{B_{Bag}} = 65\,\mathrm{MeV/fm^3}$ and the magnetic field in the range of $B = 0$ to $B = 10^{18}$ G, with steps of 1×10^{17} G. For $B = 0$, the curve presents a maximum, at whose left R decreases with E_c. Such behavior is kept for relatively weak fields $B \leqslant 3 \times 10^{17}$ G. Yet, for magnetic fields of 3–6 $\times 10^{17}$ G, there is a minimum in the R vs E_c curve, shown as dots in Fig. 4(a). Below the central energy density corresponding to the minimum, the equatorial radius increases with decreasing energy and the curve departs from the $B = 0$ behavior, thus widening the difference between the polar and the equatorial radii in a drastic way. Therefore, this minimum in R sets the maximum allowed deformation by our model, i.e., the minimum value of E_c for which our results are still reasonable. As a consequence, it provides a physical criterion to separate the regions where γ can be considered close or far from one for a given magnetic field and bag energy. In Fig. 4(b), the dots highlight the values of γ corresponding to the minimum in R for each EoS, and lower values of γ should not be considered.

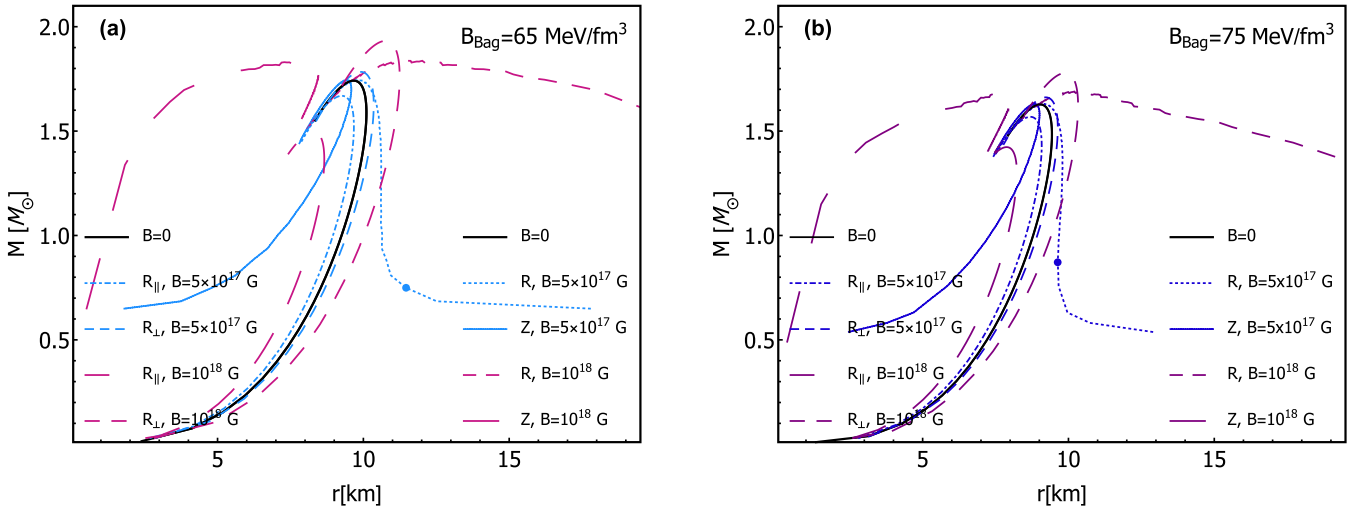

FIG. 3. Solutions for spheroidal configurations in comparison with TOV solutions and the nonmagnetized configuration at $B = 5 \times 10^{17}$ G and $B = 10^{18}$ G, where r represents both radii R and Z. (a) $B_{bag} = 65\,\mathrm{MeV/fm^3}$. (b) $B_{bag} = 75\,\mathrm{MeV/fm^3}$ [34].

For strongest magnetic fields ($\gtrsim 6 \times 10^{17}$ G), the extrema of the R vs E_c disappear, with the equatorial radius always increasing with decreasing central energy density. This explains the extremely odd behavior of the $B = 10^{18}$ G curve in Fig. 3 with respect to the spherical case and indicates that, for such magnetic fields, γ is too far from one in the low-E_c region to be admitted by our model. At higher central energy densities, even though γ gets closer to one, the model is not trusted for $B = 10^{18}$ G, and the solutions are unstable, as shown in Sec. III A.

It is interesting that other models of neutron star EoSs and structure equations also present difficulties when treating magnetic fields of the order of or higher than 10^{18} G. For example, in Ref. [20], where the anisotropy is considered through a metric in cylindrical coordinates, the metric coefficients diverge for $B \geqslant 1.8 \times 10^{18}$ G. Besides, the theoretical limit established by the Virial theorem for the maximum magnetic field that can be supported by a NS is precisely $B \simeq 10^{18}$ G [43]. Therefore, our results seem to support this limit, indicating the relevance of going deeper to better understandf the physical reasons behind it.

The effects of varying B_{Bag} and the magnetic field on the deformation of the stars can also be seen through the ellipticity, defined as [29]

$$\epsilon = \sqrt{1 - \gamma}. \tag{14}$$

In the spherical case, $\gamma \to 1$ and $\epsilon \to 0$, while for the most deformed stars, $\gamma \to 0$ and $\epsilon \to 1$. In Fig. 5 we show the ellipticity ϵ as a function of the mass and the central energy density and show that the increase in the magnetic field and in B_{Bag} leads to a greater deformation of the star.

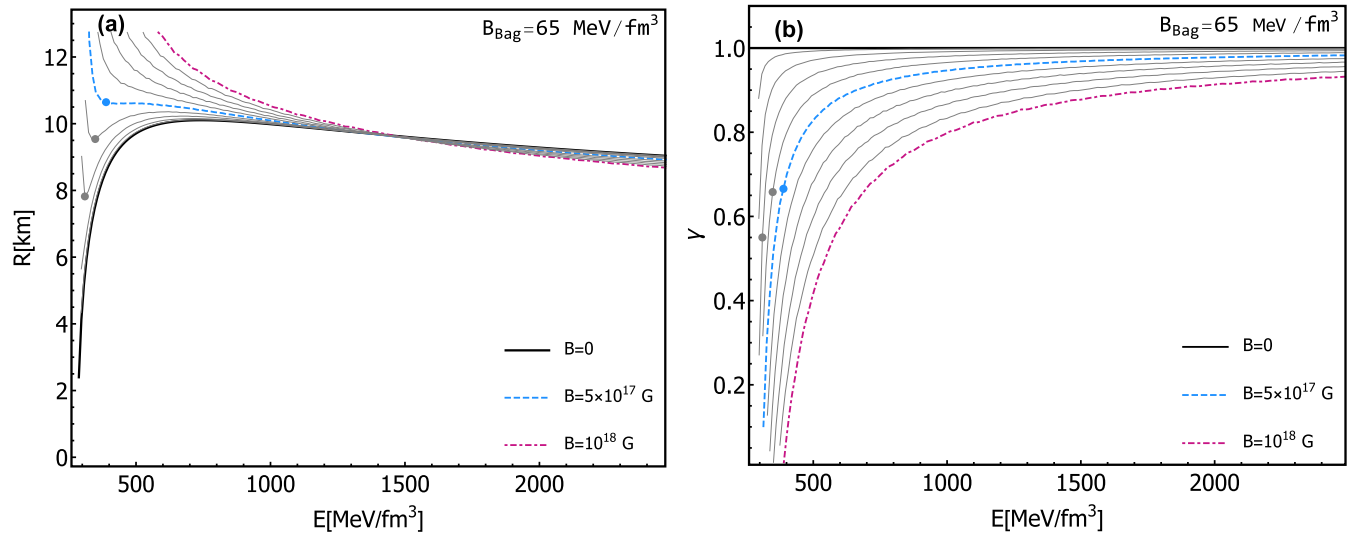

FIG. 4. Equatorial radius (a) R and (b) γ as a function of the central energy density for $B_{bag} = 65\,\mathrm{MeV/fm^3}$. The gray lines correspond to different values of the magnetic field between $B = 10^{17}$ G and $B = 10^{18}$ G, taking steps of 1×10^{17} G.

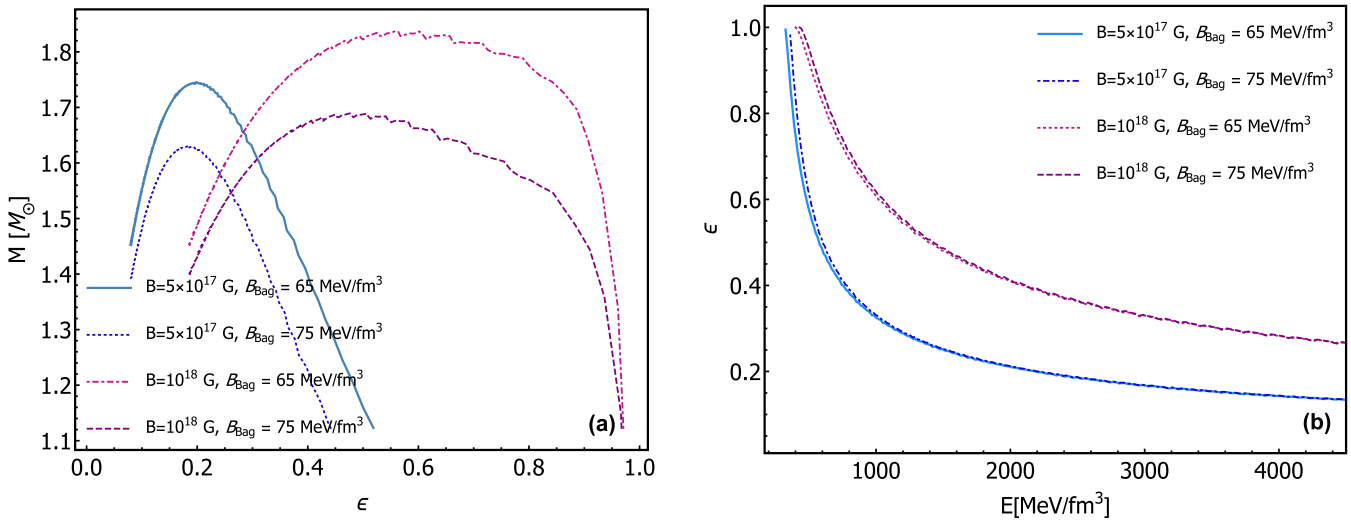

FIG. 5. Elipticity ϵ as a function of (a) mass M and (b) energy density E at $B = [0, 5 \times 10^{17}, 10^{18}]$ G and for fixed values of $B_{Bag} = [65\,\mathrm{MeV/fm^3}, 75\,\mathrm{MeV/fm^3}]$.

A. Stability of the solutions of the γ equations

The mass-radii curves obtained for SSs with Eqs. (13) correspond to stellar configurations in hydrostatic equilibrium [44]. However, equilibrium does not necessarily imply stability [22,45]. To find which of those solutions represents stable COs we use two criteria. The first is related to the stability with respect to radial oscillations and requires that $dM/dE_c > 0$ [22,46], so the CO will not fall apart. Although this is the usual stability condition corresponding to isotropic stars, stability studies of some anisotropic systems shows that it may hold for some nonspherical stars [47–49]. Here, we apply it to our model based on the assumption that, for the validity of the γ equations, the deviation from the spherical shape must be small and from a formal point of view there is a similitude between this structure equation and the TOV equations.

The second stability criterion requires the star's gravitational mass (the one calculated with the structure equations) be lower than its baryonic mass M_B, which is the sum of the masses of all its particles. This last criterion is applied to guarantee the stability of the CO with respect to the dispersion of the matter that composes it [45].

In Fig. 6(a) the mass has been plotted as a function of the central energy density. The points represent the maximum of each curve. Therefore, the stars to the left of the maximum are stable ($dM/dE_c > 0$), while those to the right are not ($dM/dE_c < 0$) and must be discarded. For fixed magnetic field, increasing B_{Bag} increases the stability region, whereas, for a fixed B_{bag}, increasing B reduces it.

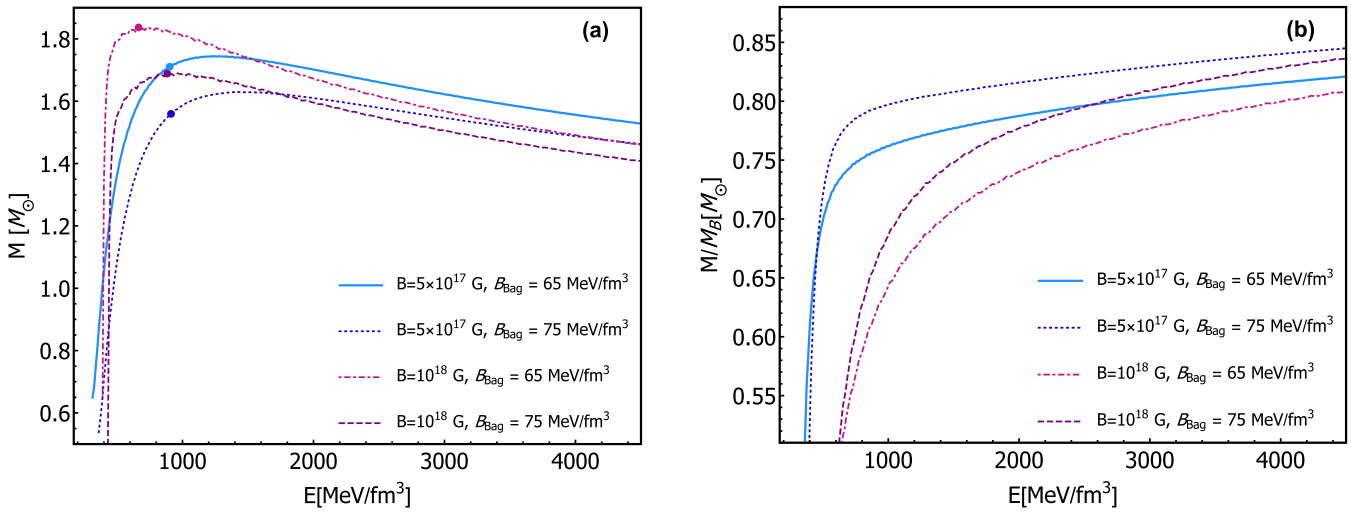

FIG. 6. Mass M as function of (a) energy density E and (b) ratio between M and the baryon mass M_B at $B = [0, 5 \times 10^{17}, 10^{18}]$ G and for fixed values of $B_{Bag} = [65\,\mathrm{MeV/fm^3}, 75\,\mathrm{MeV/fm^3}]$.

TABLE II. Maximum values of masses M (13) and the corresponding radius R, Z, and γ parameter.

B (G)	B_{Bag} (MeV/fm^3)	M ($M_\odot$)	R (km)	Z (km)	γ
5×10^{17}	65	1.74	9.79	9.41	0.96
	75	1.62	9.16	8.84	0.96
10^{18}	65	1.83	12.01	7.66	0.63
	75	1.68	10.20	7.88	0.77

To apply the second stability criterion we start from the definition of the baryonic mass M_B [50]:

$$M_B = m_N \int_0^R \frac{4\pi r^2 n_B(r)}{[1-2Gm(r)/r]^{\gamma/2}} dr, \tag{15}$$

where m_N is the neutron mass and $n_B(r)$ is the baryonic density. The regions where $M/M_B < 1$ are stable, while those where $M/M_B > 1$ correspond to unstable stellar configurations. Therefore, these regions should also be discarded. But, as shown in Fig. 6(b), all the stellar configurations here obtained are stable with respect to this stability criterion.

The maximum masses and corresponding radii and γ are shown in Table II. Note that the solutions for $B = 10^{18}$ G are unstable with respect to radial oscillations in the range of high central energy densities [Fig. 6(a)], while they are out of the validity range of γ equations for low central energy densities, as discussed in the previous section. Therefore, in what follows, we will not calculate the observables corresponding to this value of magnetic field.

B. Comparison of the model with strange-star candidates

In this section, we compare the spheroidal static configurations obtained from γ equations with some observable data for candidates to be SSs (see Table I). Given that spheroidal SSs have two main radii, for the comparison we defined a mean radius R_m so that the sphere it determines is equal to the surface of the spheroidal star:

$$A = 2\pi R\left[R + \frac{Z}{\epsilon}\arcsin\epsilon\right], \tag{16}$$

where ϵ is the ellipticity. In this way, the radius R_m could be connected with the surface of the COs and consequently, with its emission properties [51].

Figure 7 shows our theoretical results for the masses and radii together with the observational ones for the candidates. The shaded regions are forbidden by theoretical requirements (see the legend of Fig. 7). All configurations are in the allowed region, and in the mass interval where the candidates are concentrated. In particular, the M vs R_m curves fall in the uncertainty intervals of the masses and radii of the stars 4U1608-52 and 4U1820-30 for $B_{bag} = 75$ MeV/fm^3 and $B_{bag} = 65$ MeV/fm^3, respectively. So our model is consistent with the observations.

IV. MAGNETIZED STRANGE STARS: REDSHIFT AND MASS QUADRUPOLE

A. Gravitational redshift

Gravitational redshift is one of the main effects predicted by the Theory of General Relativity and, in turn, constitutes one of its fundamental tests. The frequency of an atomic clock depends on the value of the gravitational potential at its location. So when a photon is observed from a point at a higher gravitational potential, its wavelength is redshifted.

For a spheroidal static CO, the redshift is given by [52]

$$z_{rs} = \frac{1}{\left(1-\frac{2M}{R}\right)^{\gamma/2}} - 1, \tag{17}$$

where M and R are, respectively, the mass and the equatorial radius of the CO. If $\gamma = 1$, the spherical case is recovered.

The definition of z_{rs} explicitly includes the term M/R, so its measurement can narrow these parameters. In addition, z_{rs} has a maximum at the star's maximum point of mass, so it can also be used to rule out EoSs that do not lead to observable redshifts and therefore constitutes a benchmark to evaluate the feasibility of NSs models [14]. Our results for z_{rs} are shown in Fig. 8 for TOV and γ equations solutions.

In the spherical case, the higher values for z_{rs} are obtained for the pairs $(E, P_\perp)$. In this case, for a fixed B_{Bag}, increasing

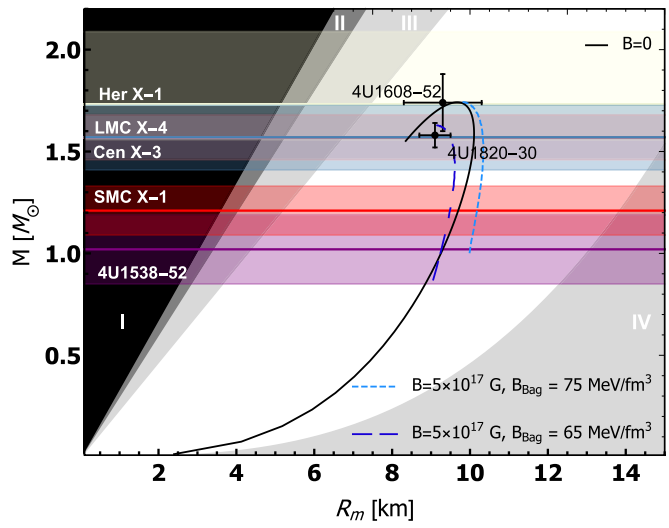

FIG. 7. Comparison of observational data for candidates of SSs with the stars obtained from Eqs. (10) and (13). The shaded regions correspond to theoretical constraints: Gravitational collapse (I); requirement of finite pressure inside the star (II); causality (III); rotational stability (IV) [25].

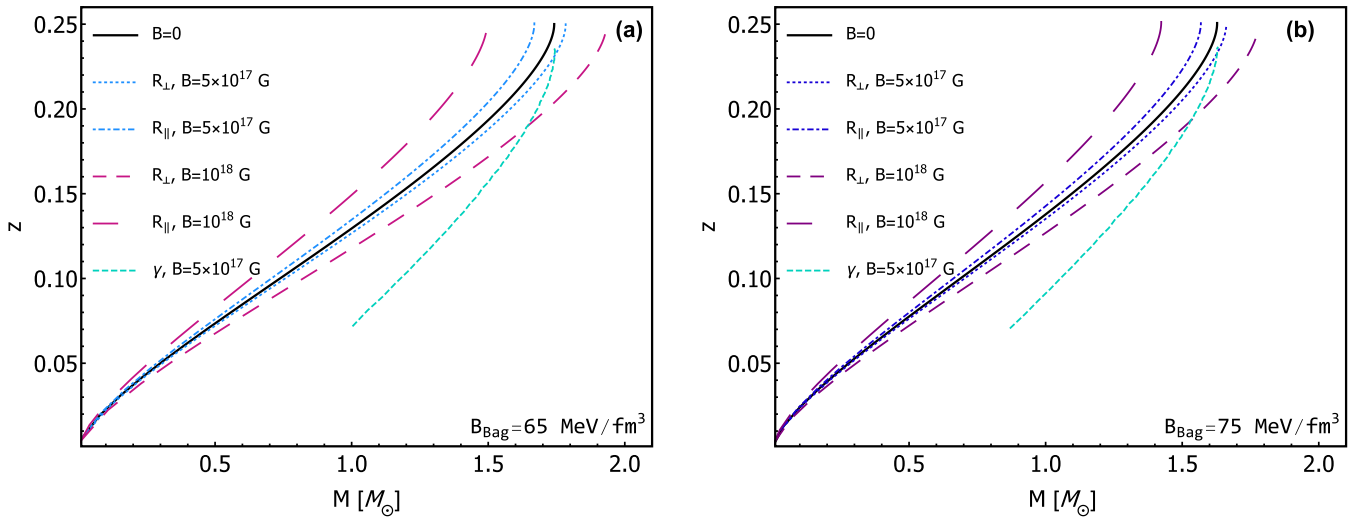

FIG. 8. Gravitational redshift z_{rs} as a function of mass M at $B = [0, 5 \times 10^{17}, 10^{18}]$ G for TOV and the γ equations. (a) $B_{Bag} = 65$ MeV/fm^3. (b) $B_{Bag} = 75$ MeV/fm^3.

the magnetic field increases z_{rs}, while changing B_{Bag} barely affects it. If we compare the results for $B = 0$ with the solutions of γ equations for $B = 5 \times 10^{17}$ G, we see that, with these, lower values of z_{rs} are obtained and the curves are far apart. This difference can be very useful to discriminate between models with and without magnetic field when comparing with observational values.

B. Mass quadrupole moment

Finally, we calculate the mass quadrupole moment of the spheroidal stars. This magnitude is directly related to the amplitude of the GWs [53], since they are only emitted in situations where an asymmetry of mass is generated that gives rise to a quadrupolar moment. Therefore, spherical stars do not have a quadrupole moment and cannot generate GWs. In contrast, magnetized stars, being deformed, have nonzero quadrupole moments that will contribute to their GWs emission. In the framework of our structure equations, the quadrupole moment of the SSs is [42]

$$Q = \frac{\gamma}{3} M^3 (1 - \gamma^2), \tag{18}$$

where $\gamma = 1$, $Q = 0$, as corresponds to the spherical case.

Figure 9 shows the SSs quadrupole moment as a function of the star mass. The oscillations in the curve are an effect of the presence of the sum by the Landau levels in the EoS. Q diminishes with B_{Bag} and its maximum is reached for stars in the region of intermediate mass and deformation. This behavior is due to the simultaneous dependence of Q on M and γ and, in particular, is determined by the fact that γ depends on the EoS and therefore varies between the stars. This result is different from that obtained in Ref. [52], where structure equations derived from the γ metric were solved by taking γ as a free parameter set by hand. In that case, since the mass quadrupole is led by the mass, its highest values are attained for the more massive stars. Therefore, connecting γ with the physics of the problem has a direct impact on the observables, which again could serve as a way to discriminate between models.

V. CONCLUSIONS

This work is a step forward in our studies about magnetized SSs [31–33]. We re-analyzed the stability of SQM under the action of a magnetic field and found that its presence reinforces the Bodmer-Witten conjecture. To compute the star's observables the EoSs have been restricted to the stability region. The macroscopic properties of the SSs—mass, radius, deformation, gravitational redshift, mass quadrupole moment—were calculated using the γ equations [30] for spheroidal compact objects. The mass-radius curves of the obtained stable configurations comply with the theoretical constraints and are consistent with the observed properties of

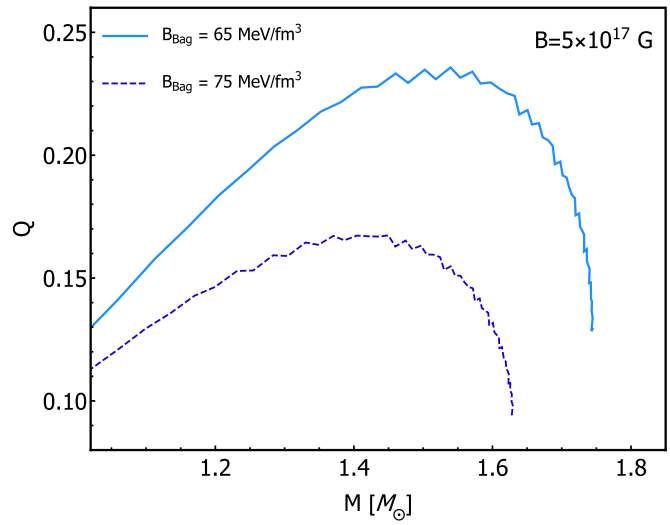

FIG. 9. Mass quadrupole moment Q as a function of mass M at $B = 5 \times 10^{17}$ G for $B_{Bag} = 65$ MeV/fm^3 and $B_{Bag} = 75$ MeV/fm^3.

SSs candidates, with masses below the observational maximum mass of neutron stars ($\approx 2M_{\odot}$) [15,54–56].

In our model, less massive stars suffer bigger deformations in contrast with the results from TOV solutions for the perpendicular and the parallel pressure independently. This reveals the model dependency of the results and highlights how important is the construction of even more realistic models. On the other hand, augmenting both $\mathrm{B_{Bag}}$ and B increases the deformation. However, the effects of changing the bag energy and the magnetic field in the stability with respect to radial oscillations of the solutions of γ equations opposes: the stability region increases with $\mathrm{B_{Bag}}$ and decreases with B. Nevertheless, none of these parameters influences the stability of the star with respect to the baryon mass criterion.

Another interesting feature of our model is that the redshift and the mass quadrupole moment depend explicitly on the deformation through the EoS—because γ appears on their mathematical expressions. As a consequence, the curve of the gravitational redshift of SSs has remarkable differences with respect to those of the spherical case. Besides, the maximum values of the mass quadrupole moment occur for the stars with intermediate values of masses and deformation, suggesting that these are the stars that should produce the most intense GWs emission, instead of those that have the maximum masses or deformation. This result is as interesting as unexpected and deserves deeper research in future work.

ACKNOWLEDGMENTS

The authors have been supported by Grant No. 500.03401 of the PNCB-MES Cuba and by the Abdus Salam International Centre for Theoretical Physics (ICTP), Trieste, Italy through the Grant of Office of External Activities (OEA) NT-09.

[1] A. R. Bodmer, Collapsed nuclei, Phys. Rev. D **4**, 1601 (1971).
[2] E. Witten, Cosmic separation of phases, Phys. Rev. D **30**, 272 (1984).
[3] N. Itoh, Hydrostatic equilibrium of hypothetical quark stars, Prog. Theor. Phys. **44**, 291 (1970).
[4] C. Alcock, E. Farhi, and A. Olinto, Strange stars, Astrophys. J. **310**, 261 (1986).
[5] S. Schramm, J. Steinheimer, V. Dexheimer, and A. Mukherjee, Modeling hybrid stars and hot matter, Nucl. Phys. A **982**, 887 (2019).
[6] M. Alford, M. Braby, M. Paris, and S. Reddy, Hybrid stars that masquerade as neutron stars, Astrophys. J. **629**, 969 (2005).
[7] M. Prakash, J. M. Lattimer, A. W. Steiner, and D. Page, Observability of neutron stars with quarks, Nucl. Phys. A **715**, 835c (2003).
[8] M. Abubekerov, E. Antokhina, A. Cherepashchuk, and V. Shimanskii, The mass of the compact object in the x-ray binary her X_{-1}/HZ her, Astron. Rep. **52**, 379 (2008).
[9] T. Gangopadhyay, S. Ray, X.-D. Li, J. Dey, and M. Dey, Strange star equation of state fits the refined mass measurement of 12 pulsars and predicts their radii, Mon. Not. R. Astron. Soc. **431**, 3216 (2013).
[10] T. Güver, F. Ozel, A. Cabrera-Lavers, and P. Wroblewski, The distance, mass, and radius of the neutron star in 4U 1608-52, Astrophys. J. **712**, 964 (2010).
[11] T. Güver, P. Wroblewski, L. Camarota, and F. Özel, The mass and radius of the neutron star in 4U 1820–30, Astrophys. J. **719**, 1807 (2010).
[12] P. Elebert *et al.*, Optical spectroscopy and photometry of SAX J1808.4-3658 in outburst, Mon. Not. R. Astron. Soc. **395**, 884 (2009).
[13] M. L. Rawls, J. A. Orosz, J. E. McClintock, M. A. Torres, C. D. Bailyn, and M. M. Buxton, Refined neutron star mass determinations for six eclipsing x-ray pulsar binaries, Astrophys. J. **730**, 25 (2011).
[14] M. Camenzind, *Compact Objects in Astrophysics* (Springer-Verlag, Berlin, Heidelberg, 2007).
[15] P. Demorest, T. Pennucci, S. Ransom, M. Roberts, and J. Hessels, Shapiro delay measurement of a two solar mass neutron star, Nature (London) **467**, 1081 (2010).
[16] F. J. Llanes-Estrada and E. Lope-Oter, Hadron matter in neutron stars in view of gravitational wave observations, Prog. Part. Nucl. Phys. **109**, 103715 (2019).
[17] E. Annala, T. Gorda, A. Kurkela, J. Nättilä, and A. Vuorinen, Evidence for quark-matter cores in massive neutron stars, Nat. Phys. **16**, 907 (2020).
[18] M. Falanga, E. Bozzo, A. Lutovinov, J. M. Bonnet-Bidaud, Y. Fetisova, and J. Puls, Ephemeris, orbital decay, and masses of ten eclipsing high-mass x-ray binaries, Astron. Astrophys. **577**, A130 (2015).
[19] E. J. Ferrer, V. de la Incera, J. P. Keith, I. Portillo, and P. L. Springsteen, Equation of state of a dense and magnetized fermion system, Phys. Rev. C **82**, 065802 (2010).
[20] D. Manreza Paret, J. E. Horvath, and A. Pérez Martínez, Anisotropic stellar structure equations for magnetized strange stars, Res. Astron. Astrophys. **15**, 975 (2015).
[21] A. Chodos, R. Jaffe, K. Johnson, C. B. Thorn, and V. Weisskopf, A new extended model of hadrons, Phys. Rev. D **9**, 3471 (1974).
[22] S. L. Shapiro and S. A. Teukolsky, *Black Holes, White Dwarfs and Neutron Stars* (John Wiley and Sons, New York, 1983).
[23] C. Thompson and R. C. Duncan, Neutron star dynamos and the origins of pulsar magnetism, Astrophys. J. **408**, 194 (1993).
[24] C. Kouveliotou, S. Dieters, T. Strohmayer, J. van Paradijs, G. J. Fishman, C. A. Meegan, K. Hurley, J. Kommers, I. Smith, D. Frail, and T. Murakami, An X-ray pulsar with a superstrong magnetic field in the soft γ-ray repeater SGR1806-20, Nature (London) **393**, 235 (1998).
[25] J. M. Lattimer and M. Prakash, Neutron star observations: Prognosis for equation of state constraints, Phys. Rep. **442**, 109 (2007).
[26] G. S. Bali, F. Bruckmann, G. Endrodi, S. D. Katz, and A. Schafer, The QCD equation of state in background magnetic fields, J. High Energy Phys. 08 (2014)177.
[27] K. Konno, T. Obata, and Y. Kojima, Deformation of relativistic magnetized stars, Astron. Astrophys. **352**, 211 (1999).
[28] D. Chatterjee, T. Elghozi, J. Novak, and M. Oertel, Consistent neutron star models with magnetic field dependent equations of state, Mon. Not. R. Astron. Soc. **447**, 3785 (2015).

[29] R. Rizaldy and A. Sulaksono, Magnetized deformation of neutron stars, J. Phys. Conf. Ser. **1080**, 012031 (2018).
[30] D. A. Alvear Terrero, V. Hernández Mederos, S. López Pérez, D. Manreza Paret, A. Pérez Martínez, and G. Quintero Angulo, Modeling anisotropic magnetized white dwarfs with γ metric, Phys. Rev. D **99**, 023011 (2019).
[31] R. G. Felipe, A. P. Martínez, H. P. Rojas, and M. Orsaria, Magnetized strange quark matter and magnetized strange quark stars, Phys. Rev. C **77**, 015807 (2008).
[32] R. G. Felipe and A. P. Martínez, Stability window and mass-radius relation for magnetized strange quark stars, J. Phys. G **36**, 075202 (2009).
[33] A. Martinez, R. Felipe, and D. Paret, Mass-radius relation for magnetized strange quark stars, Int. J. Mod. Phys. D **19**, 1511 (2010).
[34] S. L. Pérez, D. M. Paret, G. Q. Angulo, A. P. Martínez, and D. A. Terrero, Modeling anisotropic magnetized strange quark stars, Astron. Nachr. **340**, 1013 (2019).
[35] G. Quintero Angulo, A. Pérez Martínez, H. Pérez Rojas, and D. Manreza Paret, (Self-) Magnetized Bose–Einstein condensate stars, Int. J. Mod. Phys. D **28**, 1950135 (2019).
[36] A. Broderick, M. Prakash, and J. M. Lattimer, The equation of state of neutron star matter in strong magnetic fields, Astrophys. J. **537**, 351 (2000).
[37] R. Ciolfi and L. Rezzolla, Poloidal-field instability in magnetized relativistic stars, Astrophys. J. **760**, 1 (2012).
[38] A. Sur, B. Haskell, and E. Kuhn, Magnetic field configurations in neutron stars from MHD simulations, Mon. Not. R. Astron. Soc. **495**, 1360 (2020).
[39] J. Schwinger, On gauge invariance and vacuum polarization, Phys. Rev. **82**, 664 (1951).
[40] E. J. Ferrer, V. de la Incera, D. M. Paret, A. P. Martínez, and A. Sanchez, Insignificance of the anomalous magnetic moment of charged fermions for the equation of state of a magnetized and dense medium, Phys. Rev. D **91**, 085041 (2015).
[41] M. Chaichian, S. S. Masood, C. Montonen, A. Pérez Martínez, and H. Pérez Rojas, Quantum Magnetic And Gravitational Collapse, Phys. Rev. Lett. **84**, 5261 (2000).
[42] L. Herrera, F. M. Paiva, and N. Santos, The Levi-Civita space-time as a limiting case of the gamma space-time, J. Math. Phys. **40**, 4064 (1999).
[43] S. Chandrasekhar and E. Fermi, Problems of gravitational stability in the presence of a magnetic field, Astrophys. J. **118**, 116 (1953).
[44] N. K. Glendenning, *Special and General Relativity* (Springer Science + Business Media, 2007).
[45] M. Gleiser, Stability of boson stars, Phys. Rev. D **38**, 2376 (1988).
[46] S. Chandrasekhar, A general variational principle governing the radial and the non-radial oscillations of gaseous masses, Astrophys. J. **139**, 664 (1964).
[47] K. Dev and M. Gleiser, Anisotropic stars. 2. Stability, Gen. Relativ. Gravitation **35**, 1435 (2003).
[48] J. D. V. Arbañil and M. Malheiro, Radial stability of anisotropic strange quark stars, J. Cosmol. Astropart. Phys. 11 (2016) 012.
[49] K. Dev and M. Gleiser, Anisotropic stars: Exact solutions and stability, Int. J. Mod. Phys. D **13**, 1389 (2004).
[50] M. Mariani *et al.*, Magnetized hybrid stars: Effects of slow and rapid phase transitions at the hadron-quark interface, Mon. Not. R. Astron. Soc. **489**, 4261 (2019).
[51] D. Chatterjee, J. Novak, and M. Oertel, Magnetic field distribution in magnetars, Phys. Rev. C **99**, 055811 (2019).
[52] O. Zubairi, A. Romero, and F. Weber, Static solutions of Einstein's field equations for compact stellar objects, J. Phys. Conf. Ser. **615** 012003 (2015).
[53] M. Sieniawska and M. Bejger, Continuous gravitational waves from neutron stars: Current status and prospects, Universe **5**, 217 (2019).
[54] J. Antoniadis, P. C. C. Freire, N. Wex, T. M. Tauris, R. S. Lynch, M. H. van Kerkwijk, M. Kramer, C. Bassa, V. S. Dhillon, T. Driebe, J. W. T. Hessels, V. M. Kaspi, V. I. Kondratiev, N. Langer, T. R. Marsh, M. A. McLaughlin, T. T. Pennucci, S. M. Ransom, I. H. Stairs, J. van Leeuwen, J. P. W. Verbiest, and D. G. Whelan, A massive pulsar in a compact relativistic binary, Science **340**, 1233232 (2013).
[55] E. Fonseca, T. T. Pennucci, J. A. Ellis, I. H. Stairs, D. J. Nice, S. M. Ransom, P. B. Demorest, Z. Arzoumanian, K. Crowter, T. Dolch, R. D. Ferdman, M. E. Gonzalez, G. Jones, M. L. Jones, M. T. Lam, L. Levin, M. A. McLaughlin, K. Stovall, J. K. Swiggum, and W. Zhu, The nanograv nine-year data set: Mass and geometric measurements of binary millisecond pulsars, Astrophys. J. Lett. **832**, 167 (2016).
[56] H. Cromartie *et al.*, Relativistic Shapiro delay measurements of an extremely massive millisecond pulsar, Nat. Astron. **4**, 72 (2019).